Investigation of Molecular Transport and Distributions in Poly(ethylene glycol) Hydrogels with Confocal Laser Scanning Microscopy

Andrew W. Watkins[†] and Kristi S. Anseth*[,†,‡]

Department of Chemical and Biological Engineering and the Howard Hughes Medical Institute, University of Colorado, Boulder, Colorado 80309-0424

Received December 1, 2004

ABSTRACT: Confocal laser scanning microscopy (CLSM) was utilized to explore noninvasively the diffusion mechanisms of water-soluble, low molecular weight fluorescent probes in photopolymerized poly(ethylene glycol) (PEG) hydrogels. First, the simple case of 1-D diffusion in uniformly loaded PEG disks was characterized. Dye distributions in PEG disks were imaged using CLSM during release experiments and quantitatively evaluated through image analysis for comparison to Fickian diffusion models. Dye diffusion coefficients were determined by fitting Fickian diffusion equations to experimentally measured concentration profiles. Effective diffusion coefficients were on the order of 10^{-8} cm^2/s, comparing favorably to literature values. Second, the time-dependent distributions of two separate probes were monitored simultaneously to explore the multicomponent tracking capabilities of CLSM in PEG hydrogels. Finally, a more complex dye loading system was examined by embedding microparticles loaded with fluorescent dye in PEG matrices and characterizing 3-D radial dye diffusion.

Introduction

Hydrogels are currently utilized and investigated as candidates for numerous biomaterials applications, such as contact lenses, wound dressings, cell scaffolds for tissue engineering, and controlled drug delivery devices. These hydrophilic networks exhibit many desirable properties for such applications, including high levels of biocompatibility and permeability. While hydrogels can be synthesized from linear, water-soluble polymers through a variety of physical, ionic, and covalent crosslinking mechanisms, the past decade has seen increased interest in hydrogels formed via chain polymerization of high molecular weight multifunctional monomers.

With the addition of vinyl end groups to hydrophilic polymer chains, covalently crosslinked hydrogel networks are readily synthesized via photoinitiated polymerization. These photopolymerizations are very rapid, on the order of a few seconds to minutes, and can be performed with no solvent or in the presence of water at physiological temperatures. Such mild reaction conditions enable the safe encapsulation of living cells,[1−5] DNA,[6,7] and therapeutic agents.[8] In addition, the high water content of these materials allows them to mimic the physical and mechanical properties of many tissues, providing a suitable environment for cell encapsulation and subsequent tissue growth and development. As pioneered by Sawhney et al.,[9] degradable groups, such as oligo(lactic acid), can be incorporated into the macromer to enable hydrolysis of the network cross-links at physiological pH. This approach to photopolymerizable, biodegradable hydrogels has been explored fundamentally[10−12] and applied by researchers to a number of biomaterials applications, including tissue engineering[13] and controlled drug delivery.[14−16]

Many hydrogel applications are concerned with the distribution and transport of small molecules through the crosslinked networks. For example, chondrocytes encapsulated in hydrogel matrices for cartilage engineering depend on the diffusion of nutrients into the network for cell viability and the transport of cell secreted extracellular matrix components away from cells during tissue evolution.[13] Sufficient oxygen diffusion must occur in contact lenses to prevent corneal edema.[17−20] In drug delivery devices, controlling release rates of therapeutic agents is imperative in achieving proper dosing. Transport processes become increasingly difficult to predict and model for complex geometries, architectures, and loading. In addition, network degradation further complicates transport processes because diffusion coefficients may vary with time due to degradation-induced structural changes.[15] Furthermore, acidic degradation products can create pH gradients in the network which influence degradation rates, and thus solute diffusion, spatially.[21,22]

Consequently, several nondestructive approaches have been explored to characterize molecular diffusion and distributions in polymers, biomaterials, and tissues. Release/uptake experiments[15,23,24] and fluorescence recovery after photobleaching[25−28] (FRAP) are commonly used to measure diffusion coefficients but provide only a predictive measure for estimating molecular distributions. Researchers have used FTIR spectroscopic imaging and time-of-flight secondary ion mass spectrometry (TOF-SIMS) to examine molecular distributions in controlled drug release applications but are limited to surfaces and 2-D geometries.[29−31] Magnetic resonance imaging and nuclear magnetic resonance have been utilized to image controlled release tablets in 3-D with resolutions of 50−150 μm on experimentally viable time scales.[32,33]

Conversely, confocal laser scanning microscopy (CLSM) is capable of optically sectioning samples at much higher resolutions (<1 μm) with scan times on the order of a few minutes. By taking a series of 2-dimensional $x-y$ images along the z focal axis, one can compile high-resolution 3-D projections. Zhang and Chu have used confocal laser scanning microscopy to study qualitatively 3-D concentration profiles during the release of fluorescently labeled bovine serum albumin and insulin

[†] Department of Chemical and Biological Engineering.
[‡] Howard Hughes Medical Institute.
* To whom correspondence should be addressed. E-mail Kristi.Anseth@colorado.edu.

10.1021/ma0475232 CCC: $30.25
Published on Web 01/27/2005

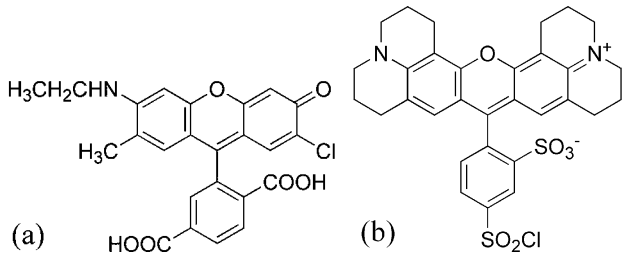

Figure 1. Chemical structures of (a) Cl-NERF (MW = 451.86 g/mol, $r_s \sim 7$ Å) and (b) Texas Red sulfonyl chloride (MW = 625.15 g/mol, $r_s \sim 7$ Å).

from hydrogels.[34,35] Other researchers have used CLSM to provide cross-sectional images of molecular distributions in polymeric microparticles[36,37] and beads.[28] Using a similar imaging technique to CLSM, Stroh et al. employed multiphoton microscopy to monitor growth factor diffusion in brain tissue.[38]

Expanding on these studies, this work explores the feasibility of applying CLSM to study molecular distributions and transport in photopolymerized poly(ethylene glycol) (PEG)-based hydrogels. The transparent nature of PEG gels makes them ideal materials for imaging embedded molecules with confocal microscopy. To explore the mechanism by which small molecules diffuse through covalently crosslinked PEG hydrogels, we examined 1-D diffusion of homogeneously loaded, low molecular weight fluorescent probes and made comparisons to theoretical Fickian models. Furthermore, we were interested in following the distributions of multiple solute species in hydrogel matrices concurrently for such applications as tracking the diffusion of multiple growth factors through a tissue engineering scaffold. To investigate the multicomponent tracking capabilities of CLSM in PEG hydrogels, the simultaneous uptake and release of two separate probes were characterized. Finally, expanding the technique to a 3-D geometry, dye release from microparticles embedded in PEG matrices was examined.

Experimental Section

Materials. Poly(ethylene glycol) diacrylate (PEG1000DA, MW = 1000) was used as received from Monomer-Polymer & Dajac Labs, Inc. (Feasterville, PA). Poly(ethylene glycol) diacrylate (PEG700DA, MW = 700) was used as received from Aldrich. The photoinitiators Irgacure 2959 (I2959) and Irgacure 651 (I651) were obtained from Ciba-Geigy and dissolved in deionized water and ethanol, respectively, to form dilute solutions. Fluorescent probes Cl-NERF (ClN, MW = 452) and Texas Red sulfonyl chloride (TxR, MW = 625), shown in Figure 1, were obtained from Molecular Probes and dissolved in deionized water to form dilute dye solutions. Using Chem3D Pro (CambridgeSoft, Cambridge, MA) to measure molecular size, both ClN and TxR have maximum dimensions of approximately 14 Å. As both dye molecules are approximately the same shape and of comparable size, one would expect similar diffusional properties.

Photopolymerization of Gel Disks. In the preparation of hydrogel disks, aqueous macromer solutions were formed by mixing PEG1000DA and PEG700DA with deionized water (DI-H_2O). Unless noted otherwise, the macromer solutions were a 50/50 wt % mixture of PEG-DA/DI-H_2O for all experiments in this paper. Using capillary action, the macromer solutions were loaded between two glass microscope slides using glass coverslips as spacers. Crosslinked networks were formed by exposing the macromer solutions to ultraviolet light (BlakRay, $\lambda = 365$ nm, intensity = 12 mW/cm^2) in the presence of a photoinitiator. Samples were polymerized for 10 min using 0.025 wt % I2959 or 1 min using 0.05 wt % I651. Differential scanning calorimetry confirmed that these exposure times were sufficient for the reactions to reach completion. Sample disks 12.5 mm in diameter and 0.4 mm in thickness were created using a stainless steel punch.

To load fluorescent probes into the gel disks, disks were placed in 3−10 μM fluorescent dye solutions, and sufficient time (>96 h) was allowed to reach equilibrium loading. Equilibrium was determined when the disks attained uniform concentration profiles.

Equilibrium Swelling. Equilibrium swelling experiments were performed by placing PEG disks ($n = 5-10$) in DI-H_2O until constant masses were attained. The disks were then patted dry and the swollen masses were recorded. Dry masses were measured after drying the disks in a vacuum oven.

Tensile Testing. Dog-bone-shaped samples were photopolymerized between glass slides using a rubber mold. Sample dimensions used were according to ASTM D638-03 type I samples for semirigid plastics. Several polymer precursor compositions were examined: PEG1000DA with 0.025 wt % I2959, PEG700DA with 0.025 wt % I2959, PEG700DA with 0.05 wt % I651, and PEG700DA with no DI-H_2O and 1.0 wt % I2959. Prior to testing, samples were swollen in DI-H_2O for 24 h. Tensile tests were performed until fracture, five samples per composition, using an MTS Synergie 100 material tester (MTS, Eden Prairie, MN) with 10 N load cell and a cross-head speed of 5 mm/min.

Dye Release Studies. Dye-loaded polymer disks were placed in vials containing 10 mL of DI-H_2O and gently shaken. The high diameter to thickness aspect ratio (~25) of the disks was selected to approximate one-dimensional diffusion in the z-direction by assuming radial diffusion to be negligible. The disks were placed in fresh solvent every 5 min for the first 30 min and then every 15 min until 2 h had passed in order to maintain sink conditions. The solvent was then changed every few hours for at least 48 h until dye release had completed. The probe quantity released in the vials was monitored using fluorescence intensity that was calibrated to probe concentration using a Wallac Victor^2 1420 multilabel counter. All release experiments were performed at room temperature and repeated three times ($n = 3$).

At predetermined time points, 3-dimensional image stacks, spanning the thickness of the dye release disks, were captured using a Zeiss Pascal LSM 5 confocal microscope (Carl Zeiss, Thornwood, NY). ClN was excited using the 488 nm line of an argon ion laser, and the fluorescence was collected using a 520 nm long-pass filter. Texas Red was excited with a 543 nm helium−neon laser, and fluorescence was collected with a 560 nm long-pass filter. Each image stack required approximately 1.5−2 min to capture. Images were captured as 512 × 512 pixels with a pixel size of 1.8 μm and as slices approximately 12−20 μm thick. Improved z-resolution can be achieved but was sacrificed to shorten imaging times. Image stacks were analyzed using ImageJ software, which is distributed by the National Institutes of Health. Dye concentration was found to have a linear relationship with emission intensity for the range of concentrations used in these studies.

When quantifying emission of fluorescent probes, photobleaching is a major source of concern. In this study, TxR and ClN were chosen due to their relative photostability when compared to other dyes. To validate this conjecture, gels loaded with these dyes were excited by laser at the appropriate wavelengths for six z-stack cycles (2 min/cycle) and monitored for changes in emission intensity ($n = 3$). Upon statistical analysis using ANOVA, no statistically significant difference ($\alpha = 0.05$) between initial and final emission intensities was seen for either of the dyes.

Additionally, depth-dependent signal attenuation can be problematic in CLSM imaging, particularly in quantitative analysis. Attenuation can be attributed to number of factors, including mismatches in refractive index, light scattering, diffraction, and absorption.[39] In this work, signal attenuation was found to be negligible for the sample thicknesses (<400

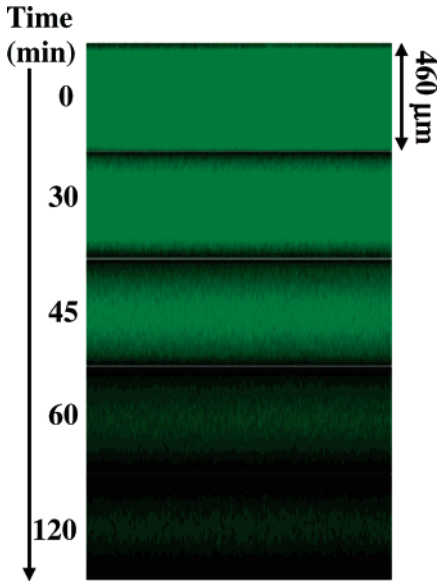

Figure 2. Time series of cross-sectional $x-z$ planes for release of Cl-NERF from PEG1000DA demonstrating dye distribution evolution with time.

Table 1. Swelling, Number Average Molecular Weight between Cross-Links, and Calculated Average Mesh Sizes for PEG Gels

macromer	processing conditions	Q	$\bar{M}_c$ (g/mol)	ξ (Å)
PEG1000DA	50 wt % H_2O 0.025 wt % I2959	3.34 ± 0.03	2360	60
PEG700DA	50 wt % H_2O 0.025 wt % I2959	2.21 ± 0.03	990	30
PEG700DA	50 wt % H_2O 0.05 wt % I651	2.21 ± 0.03	1080	30
PEG700DA	0 wt % H_2O 1.0 wt % I651	1.61 ± 0.01	470	20

μm) and fluorescent dye concentrations (3−10 μM) used but became apparent in PEG gels thicker than approximately 500 μm.

Theoretical Calculations. All theoretical calculations were performed using MATLAB (The MathWorks, Natick, MA). Theoretical equations were fit to experimental data using nonlinear least-squares regressions with the MATLAB Curve Fit Toolbox. Infinite summations were carried out to $n = 1000$, though $n = 10-15$ was sufficient in most cases.

Preparation of Poly(ethylene glycol) Diacrylate Microparticles. Spherical PEG microparticles were prepared utilizing a suspension polymerization technique in light mineral oil. A 1 mL solution of PEG700DA and 1 wt % I651 was slowly injected by hand from a 1 mL syringe fitted with a 26 gauge needle into a 40 psi stream of nitrogen gas. The nitrogen gas stream dispersed droplets of the PEG solution into a 400 mL beaker containing 100 mL of light mineral oil (Aldrich) stirring rapidly. The mineral oil solution was then immediately placed under ultraviolet light (BlakRay, $\lambda = 365$ nm, intensity = 12 mW/cm^2) for 20 s and removed, all while constantly stirring. The resulting microparticles were vacuum-filtered and rinsed five times with deionized water. The particles were then lyophilized for 24 h and separated by size using phosphor bronze sieves. For loading with fluorescent dye, particles less than 180 μm in diameter were placed in a phosphate buffered saline solution of 10 μM TxR sulfonyl chloride for at least 48 h prior to usage.

Microparticles Embedded in PEG Disks. Microparticles were vacuum-filtered to remove excess dye solution and then placed in PEGDA solutions at 1 mg/mL microparticle/macromer solution. The microparticle/macromer solution was then vortexed for several seconds to disperse the microparticles homogeneously. PEG disks were produced via photopolymerization as described above. Polymerized disks were placed in DI-H_2O, and individual microparticles were monitored over time by capturing CLSM image stacks at predetermined time points. Images were captured with 1.8 μm lateral and vertical resolutions.

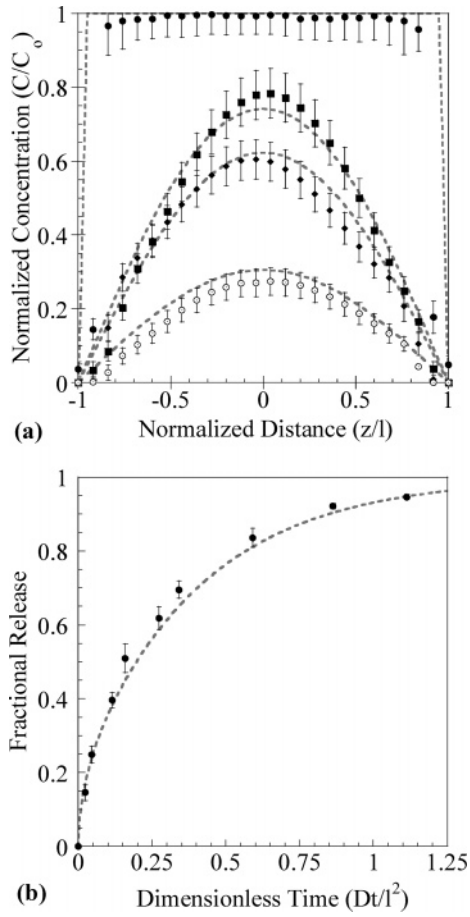

Figure 3. (a) Experimental (markers) and theoretical (dashed lines) concentration profiles for release of Cl-NERF from PEG1000DA: ●, 0 min ($Dt/l^2 = 0$); ■, 45 min ($Dt/l^2 = 0.21$); ◆, 60 min ($Dt/l^2 = 0.29$); ○, 120 min ($Dt/l^2 = 0.57$). z/l represents the dimensionless distance from the vertical center of the disk, where −1 is the top surface and 1 is the bottom surface. (b) Corresponding experimental (markers) and theoretical (dashed lines) cumulative fractional release profiles with the y-axis normalized to the total dye initially loaded in the disk. $D_{Cl-NERF} = 4.2 \times 10^{-8}$ cm^2/s was used for theoretical calculations.

Table 2. Diffusion Coefficients Calculated from Least-Squares Nonlinear Regression of Concentration Profiles (D_{CP}) and Fractional Release Data (D_{FR})

probe	macromer	D_{CP} (cm^2/s × 10^8)	D_{FR} (cm^2/s × 10^8)
Cl-NERF	PEG1000DA	4.2 ± 0.6[a]	4.5 ± 0.5[a]
Texas Red SC	PEG1000DA	7.7 ± 0.9[a]	7.4 ± 0.3[a]
Cl-NERF	PEG700DA	4.5 ± 0.6	3.5 ± 0.6
Texas Red SC	PEG700DA	4.2 ± 0.9	3.2 ± 0.3

[a] Statistically significant differences between diffusion coefficients for ClN and TxR in PEG1000DA.

Statistical Analysis. All data are reported as mean values plus or minus standard deviation. Single factor analysis of variance (ANOVA) was performed to characterize statistical significance between data ($\alpha = 0.05$).

Results and Discussion

Network Structure. There are several factors that affect rates of diffusion in hydrogels, including the size of the diffusing solute relative to the mesh size of the network. To tailor diffusion rates in these PEG gels, one

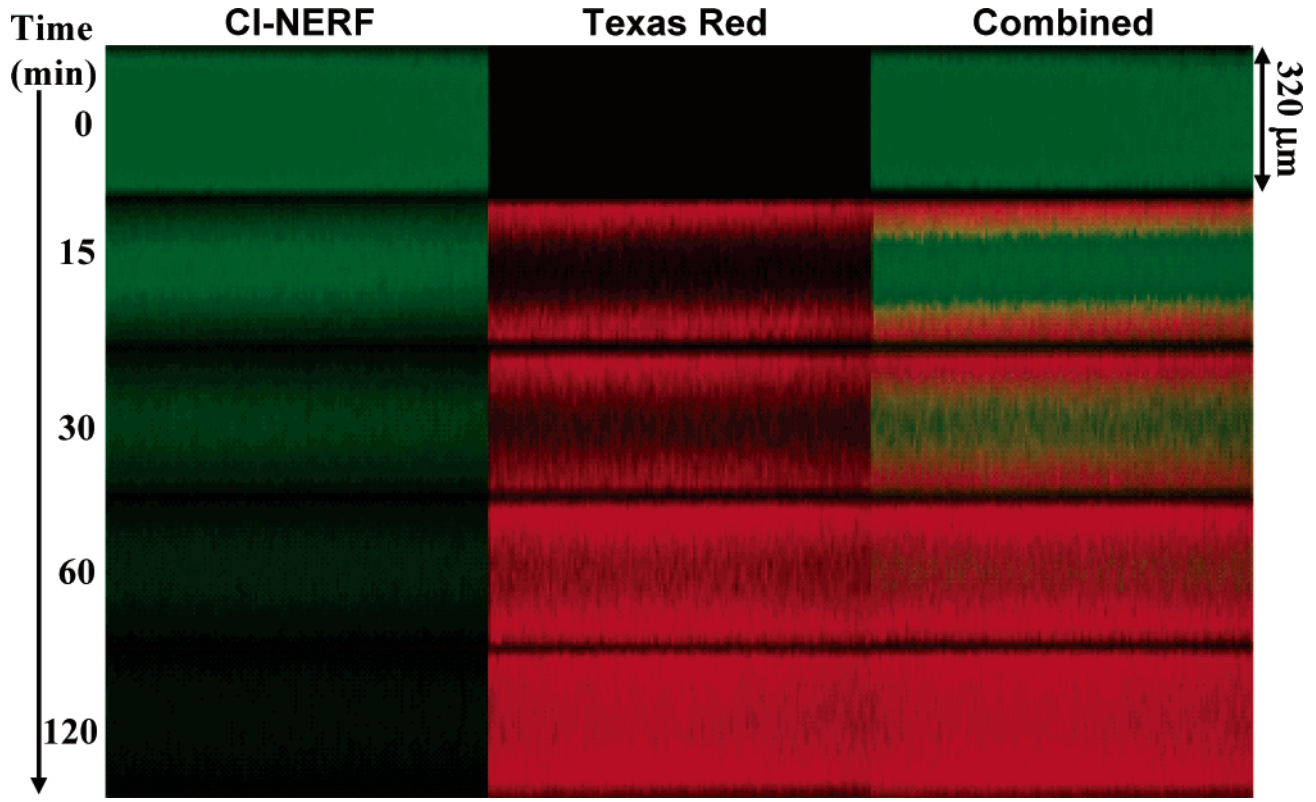

Figure 4. Time series of cross-sectional $x-z$ profiles of simultaneous release of Cl-NERF and uptake of Texas Red using a Cl-NERF loaded PEG700DA disk in an aqueous Texas Red solution.

can control the hydrogel mesh size by varying the molecular weight of the macromer precursor. Additionally, the mesh size is dependent on processing conditions, such as initiation rate and solvent concentrations. In this work, the initiation rate and solvent concentrations were held constant, while two different PEG macromer molecular weights were investigated, 700 and 1000. In the subsequent embedded microparticle studies, processing conditions were varied to further control diffusional properties. Equilibrium swelling experiments were performed on all networks investigated to determine structural differences between gels.

To estimate gel mesh sizes, the equilibrium mass swelling ratio (q), the ratio of swollen to dry mass, was measured and converted to the equilibrium volume swelling ratio (Q) through the densities of the PEG and water.[40] From these equilibrium swelling experiments and tensile testing data, the average molecular weight between cross-links ($\bar{M}_c$) was estimated using relationships based on rubber elasticity theory, neglecting chain end effects.[40−42]

$$\frac{1}{\bar{M}_c} = \frac{Q^{1/3}}{RT\rho_p}\left(\frac{\bar{r}_i^{\,2}}{\bar{r}_0^{\,2}}\right)^{-1}\frac{\tau}{\alpha - 1/\alpha^2} \qquad (1)$$

In this relationship, ρ_p is the density of the polymer, R is the gas constant, T is temperature, $\bar{r}_i^2/\bar{r}_0^2$ is the ratio of end-to-end distance in the real network vs the end-to-end distance of isolated chains (approximated as 1), τ is the tensile stress, and α is the extension ratio ($\alpha = 1 + \epsilon$, where ϵ is strain).

Using the calculated $\bar{M}_c$, a mesh size (ξ) can be estimated using the method described by Canal and Peppas (eq 2).[43] Here, C_n is the characteristic ratio of the polymer, n is the number of bonds between cross-links, and l is the average bond length within the repeat unit.

$$\xi = v_2^{\,-1/3} C_n^{\,1/2} l n^{1/2} \qquad (2)$$

Swelling and mesh size results are summarized in Table 1. Using similar processing conditions, gels made from PEG1000DA ($Q = 3.34 \pm 0.03$) exhibited significantly higher volume swelling ratios than those made from PEG700DA ($Q = 2.21 \pm 0.03$). Correspondingly, the estimated average mesh size for PEG1000DA was approximately twice that of PEG700DA, 60 to 30 Å, respectively, which implies diffusion in the PEG1000DA gels will be faster. Note that these calculations are merely estimates, as these relatively highly crosslinked networks are heterogeneous in their structure and exhibit nonidealities, such as those associated with cyclization, which further impact the cross-linking density calculation. In examining the effects of processing conditions on the gel structures, networks formed from 50/50 wt % PEG700DA/DI-H_2O with 0.025 wt % I2959 demonstrated identical swelling properties to those formed from 50/50 wt % PEG700DA/DI-H_2O with 0.05 wt % I651, while gels formed from PEG700DA with no water and 1 wt % I651 had significantly lower volume ratios and mesh sizes.

CLSM Characterization of Diffusion in 1-D. To investigate diffusion mechanisms for low molecular weight molecules and to validate CLSM as a technique for measuring molecular distributions in PEG hydrogels, the simple case of 1-D diffusion in uniformly loaded disks was first examined. Dye release studies were performed with macromer/dye combinations of PEG1000DA/ClN, PEG1000DA/TxR, PEG700DA/ClN, and PEG700DA/TxR. For each combination, image stacks were captured to quantify concentration profiles

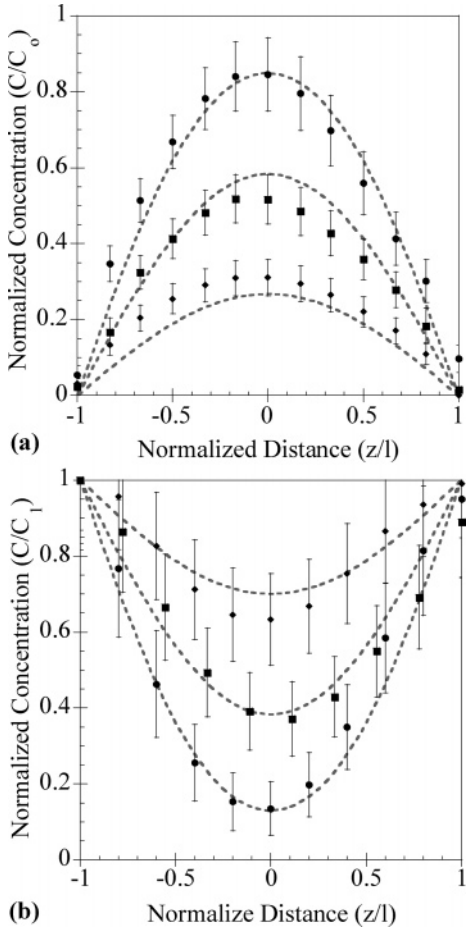

Figure 5. Experimental (markers) and theoretical (dashed lines) concentration profiles for simultaneous (a) release of Cl-NERF and (b) uptake of Texas Red in PEG700DA disk; $D_{\text{Cl-NERF}} = 4.5 \times 10^{-8}$ cm^2/s and $D_{\text{TexasRed}} = 4.2 \times 10^{-8}$ cm^2/s were used for theoretical calculations. Corresponding Dt/l^2 values for Cl-NERF/Texas Red: ● (15 min) = 0.16/0.15, ■ (30 min) = 0.32/0.29, ◆ (60 min) = 0.63/0.59. z/l represents the dimensionless distance from the vertical center of the disk, where −1 is the top surface and 1 is the bottom surface.

in the $x-z$ plane at several time points, and cumulative release was monitored for three separate disks. For comparison, the diffusion of solute in PEG was calculated using solutions to Fick's second law of diffusion (eq 3) for a planar sheet with the initial condition of uniform initial concentration ($C = C_0$, $-l < z < l$, $t = 0$), the boundary condition of surface concentrations equal to zero assuming sink conditions ($C = 0$, for $z = -l$ and $z = l$, $t \geq 0$), and assuming a constant diffusion coefficient.[44]

$$\frac{\partial C}{\partial t} = D\,\frac{\partial^2 C}{\partial z^2} \tag{3}$$

Using separation of variables, an exact analytical solution is achieved, shown in eq 4.

$$\frac{C - C_0}{C_1 - C_0} = 1 - \frac{4}{\pi} \times \sum_{n=0}^{\infty} \frac{(-1)^n}{2n+1} \exp\left\{-D(2n+1)^2 \frac{\pi^2 t}{4l^2}\right\} \cos\left[\frac{(2n+1)\pi z}{2l}\right] \tag{4}$$

The corresponding cumulative fractional release or the amount of solute released relative to total solute loaded in a disk is defined in eq 5.

$$\frac{M_t}{M_\infty} = 1 - \sum_{n=0}^{\infty} \frac{8}{(2n+1)^2\pi^2} \exp\left\{-D(2n+1)^2 \frac{\pi^2 t}{4l^2}\right\} \tag{5}$$

Representative of images captured during dye release, shown in Figure 2 is a time series of cross-sectional $x-z$ planes during the release of ClN from PEG1000DA illustrating the formation of concentration gradients. Upon quantification through image analysis, Fickian profiles (eq 5) were fit to the experimentally measured concentration profiles to estimate diffusion coefficients at each time point. The R^2 values for fitted curves ranged from 0.91 to 0.97. Experimental error may be introduced because of the short time scale of the experiment and imperfect mixing resulting in nonsink conditions.

The effective diffusion coefficients for each combination were calculated by averaging the diffusion coefficients of at least three time points in each disk and then averaging values for the three disks plus or minus the standard deviation between disks. Estimated diffusion coefficients were then substituted into the Fickian diffusion solutions to calculate concentration and release profiles. In Figure 3a, time-dependent experimental and theoretical normalized dye concentrations are plotted with respect to spatial position in a ClN-PEG1000DA gel sample. The corresponding experimental and theoretical cumulative fractional release profiles plotted with respect to dimensionless time (Dt/l^2) are shown in Figure 3b. Typical of results seen in release studies for both probes, the experimentally measured concentration profiles in Figure 3a demonstrate parabolic shapes characteristic of Fickian diffusion. The representative concentration and cumulative fractional release profiles in Figure 3a,b exhibit good agreement between experimentally measured and theoretically predicted results, further suggesting that a Fickian diffusion mechanism is present. Similar agreement was seen for studies using PEG700DA and TxR (results not shown). The most pronounced deviations between experimental and theoretical results were seen in the initial concentration profiles at the surfaces of the disk. This was attributed to several factors. First, though the imaging process takes only 1.5−2 min, the rapid rate of concentration driven diffusion at early time points may result in an appreciable change in dye concentration during imaging. Moreover, because of the z-resolution used (approximately 12 μm), image slices at the surface will likely overlap the interface between polymer disk and glass coverslip or microscope slide, resulting in a lower than expected signal reading. In addition, the change in refractive index at the polymer−glass interface may cause some image distortion. Finally, the structure of the gel at the surfaces may vary slightly from the bulk, resulting in a disparity in equilibrium loading.

For comparison, diffusion coefficients were also estimated by fitting eq 5 to cumulative release data. R^2 values for fitted curves ranged from 0.93 to 1.00. A comparison of the calculated diffusion coefficients is shown in Table 2. There was no statistical difference between diffusion coefficients calculated from concentration profile data and those calculated from cumulative release data for any of the dye/macromer combinations. The diffusion coefficients calculated from concentration profiles exhibited slightly higher standard de-

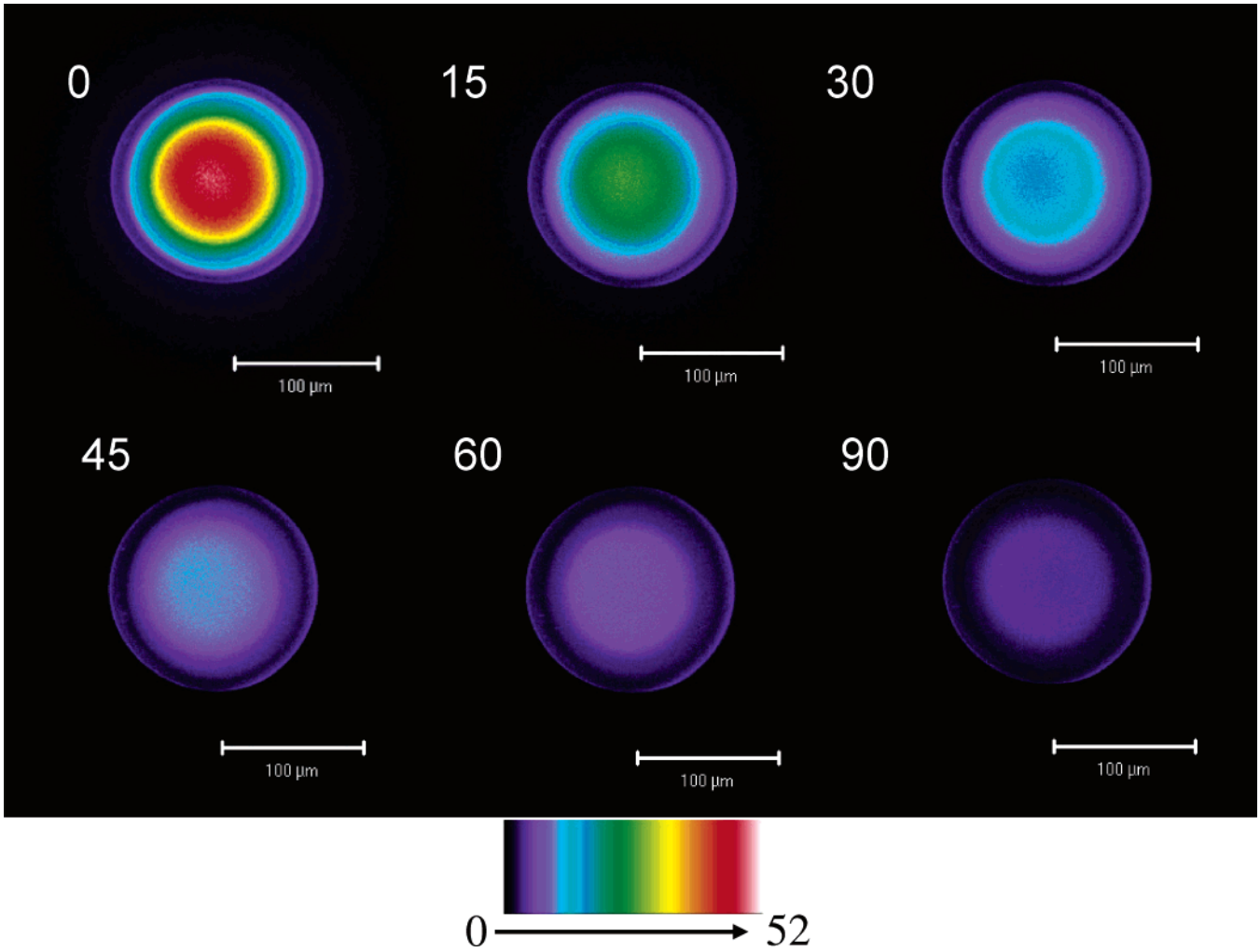

Figure 6. Time series of 3-D projections of PEG700DA microparticle loaded with Texas Red embedded in PEG700DA disk formed using 0.1 wt % I651. Times are given in minutes, and false color intensity represents Texas Red concentration, with a maximum of 52 μM.

viations, suggesting the technique may be better suited for qualitative analysis.

By assuming spherical geometries for the dye molecules, diffusion coefficients can be estimated for dilute solutions using the Stokes−Einstein equation (eq 6).

$$D_0 = \frac{k_B T}{6\pi\eta r_s} \tag{6}$$

In this equation, k_B is Boltzmann's constant, T is temperature, η is the viscosity of water, r_s is the hydrodynamic radius of the solute, conservatively assumed to be one-half of the maximum dimension for TxR and ClN (7 Å), and D_0 is the solute diffusivity in water at T. Substituting the appropriate values into eq 6, the diffusion coefficient for the two dye molecules in water was estimated to be 3.5×10^{-6} cm^2/s. As the gels studied in this work are highly crosslinked and the diffusing solutes are of approximately the same size scale as average mesh size, one would expect diffusion in the gels to be moderately hindered in comparison to diffusion in free solution.

Therefore, the estimated diffusion coefficients on the order of 10^{-8} cm^2/s appear reasonable. Additionally, these values compared favorably to reported literature values of 1.4×10^{-8} cm^2/s for tetramethyl isothiocyanate (MW = 444 g/mol) in PEG1000 dimethacrylate[45] and

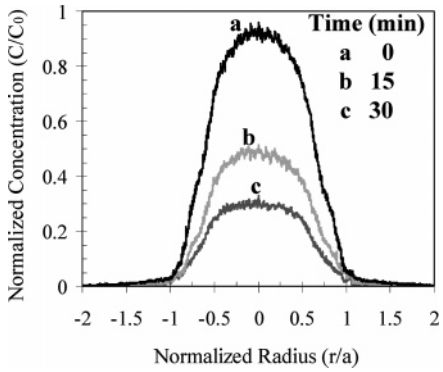

Figure 7. Time series of measured concentration profiles of PEG700DA microparticle loaded with Texas Red embedded in PEG700DA disk formed using 0.1 wt % I651. Normalized radius is the ratio of the distance from the center of the microparticle, r, to the radius of the microparticle, a, where −1 and 1 represent the sphere walls.

$(3.54-4.24) \times 10^{-9}$ cm^2/s for acid orange 8 (MW = 364 g/mol) in crosslinked poly(hydroxyethyl methacrylate).[46] Scott and Peppas reported similar values for diffusion of proxyphylline (MW = 238 g/mol) in comparable crosslinked PEGDA systems.[47]

Comparing values estimated in this study, the diffusion coefficients for TxR were significantly higher in PEG1000DA than in PEG700DA, which was predicted

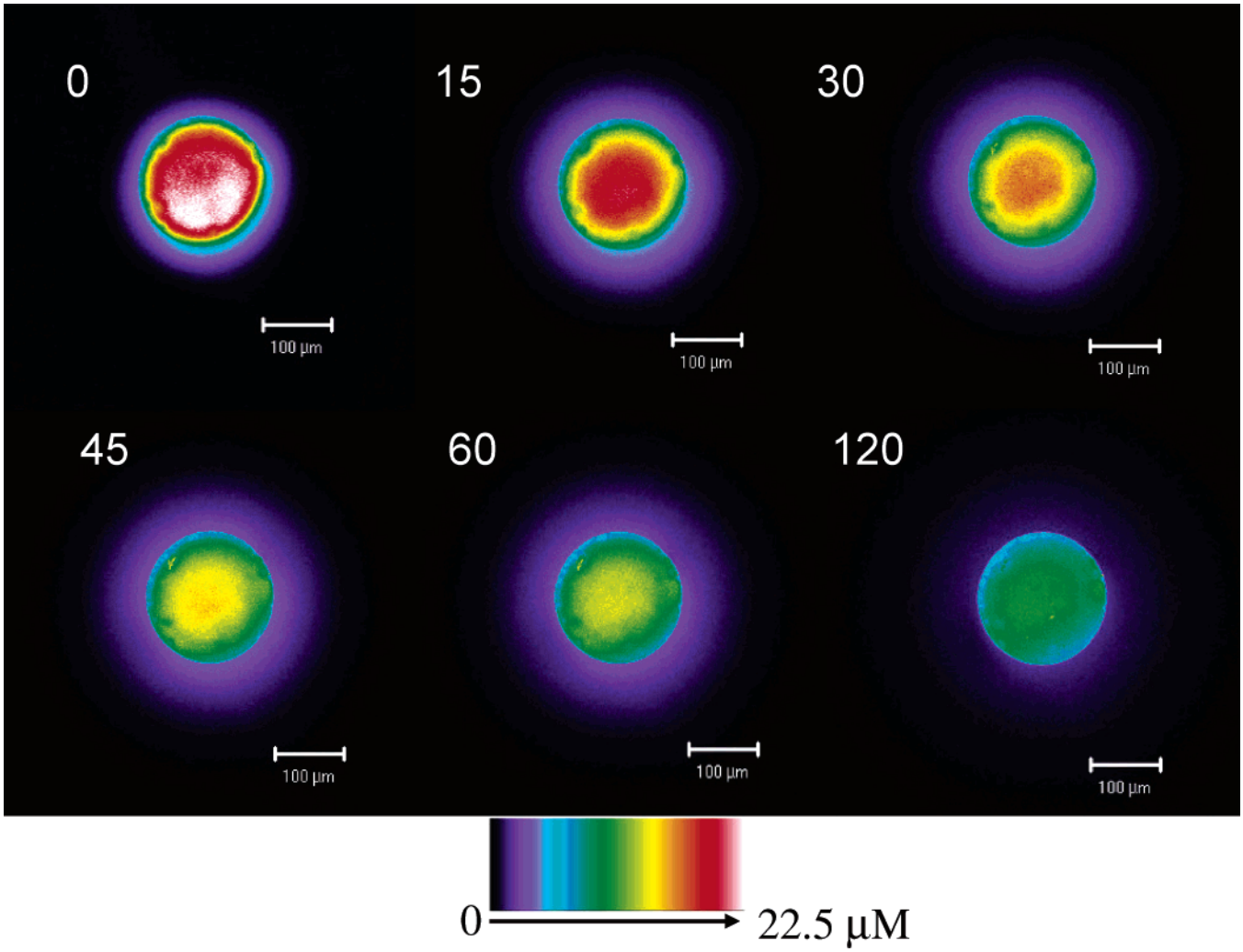

Figure 8. Time series of 3-D projections of PEG700DA microparticle loaded with Texas Red embedded in PEG700DA disk formed using 1.0 wt % I651. Times are given in minutes, and false color intensity represents Texas Red concentration, with a maximum of 22.5 μM.

by the differences in mesh size. Interestingly, there were no statistically significant differences between ClN diffusion coefficients in PEG700DA and PEG1000DA, which may reflect the qualitative nature of this technique. TxR and ClN diffusion coefficients were statistically equivalent in PEG700DA, as would be expected for molecules of similar size and structure.

Multicomponent Diffusion. One major advantage of CLSM is the ease of monitoring multiple components simultaneously. By using probes with distinct excitation and/or emission spectra, it is possible to distinguish between the fluorescence outputs of two or more probes. To investigate this capability, the simple system of 1-D diffusion in disks was again examined. PEG700DA disks were loaded with ClN and then placed in dilute aqueous solutions of TxR to simultaneously monitor ClN release and TxR uptake. While there is some overlap in the emission and excitation of these two probes, they were readily separated by exciting ClN at a lower wavelength, 488 nm compared to 543 nm, and using emission filters (505−600 nm band-pass for ClN, 650 nm long pass for TxR) to separate emission yields. The disk was confocally imaged at several time points. A time series of cross-sectional $x-z$ images for each individual dye channel, as well as the combined channels, is shown in Figure 4, illustrating the dynamic concentration gradients for both probes.

Using diffusion coefficients estimated in the single probe release experiments, theoretical concentration profiles were calculated using the Fickian solutions described previously. Uptake of TxR was calculated using eq 4 with an initial concentration of $C_0 = 0$ and constant surface concentrations ($C = C_1$ for $z = -l$ and $z = l$, $t \geq 0$). In Figure 5, time-dependent experimental and theoretical normalized dye concentrations are plotted with respect to spatial position for the multicomponent release study. Upon comparison, one notes that the theoretically predicted profiles shown in Figure 5 are consistent in shape and magnitude to the experimentally imaged profiles for both ClN and TxR.

Monitoring Dye Release from Embedded Microparticles. To study and characterize what happens in a more complex initial dye distribution, dye-loaded PEG microparticles were photoencapsulated in PEG matrices to create a 3-D release environment. In the first case, the PEG microparticles were formed from a 100/0 wt % PEG700DA/DI-H_2O solution using 1.0 wt % I651 ($\xi \sim$ 20 Å), and the embedding network was formed from a 50/50 wt % PEG700DA/DI-H_2O solution using 0.05 wt % I651 ($\xi \sim$ 30 Å). As shown in Figure 6, a time series of 3-D projections of a single microparticle embedded in the PEG gel, concentration gradients developed within the microparticles, but no appreciable concentration was seen beyond the walls of the microspheres. The

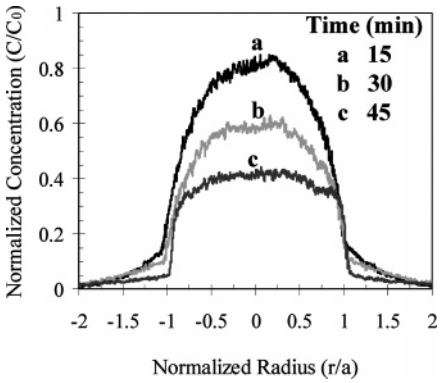

Figure 9. Time series of measured concentration profiles of PEG700DA microparticle loaded with Texas Red embedded in PEG700DA disk formed using 1.0 wt % I651. Normalized radius is the ratio of the distance from the center of the microparticle, r, to the radius of the microparticle, a, where -1 and 1 represent the sphere walls.

images were quantitatively analyzed by averaging five radial concentration profiles through the center of the particles. The quantitative results shown in Figure 7 confirm the visual interpretation, showing no concentration gradient outside of the sphere despite a declining concentration within the sphere. This can be attributed to a higher rate of diffusion in the PEG matrix than in the microparticles. The higher initiator concentration and no solvent condition used in the production of the microparticles resulted in a smaller mesh size, thus causing a slower rate of diffusion relative to the embedding matrix. The parabolic shape of the concentration profiles again points to a Fickian diffusion mechanism.

In the second case, the embedding network was formed from the same macromer precursor solution as was used in the preparation of the microparticles (no DI-H_2O, 1 wt % I651, $\xi \sim 20$ Å). Ideally, the diffusive properties of TxR in the matrix and the microparticles will be matched. As shown in Figure 8, a time series of 3-D projections of a single microparticle, a measurable concentration of TxR was detected outside of the microparticles. Quantitative analysis of radial concentration profiles confirmed this elucidation (Figure 9), as concentrations as high as 15% of the initial microparticle loading were observed external to the particles. By increasing the cross-linking density in the surrounding network, the diffusion of the dye molecules is sufficiently obstructed to enable the development of a detectible gradient external to the particle wall. Moreover, the flattening of the concentration profiles within the particles over time suggests that rate of diffusion in the PEG network outside of the particles is actually the limiting factor for dye release. Though the microparticle and embedding network precursor compositions were identical, the difference in polymerization conditions has resulted in a noticeable disparity in cross-linking densities.

Polymeric microparticles have been well established in the field of controlled drug delivery for many years. More recently, several researchers have investigated microparticles as delivery vehicles embedded in tissue engineering scaffolds as a method for sustained delivery of active agents, such as proteins and polypeptides, which influence cell behavior.[48,49] Typically, the global effect of the active agent is investigated. The CLSM technique demonstrated in this work can provide insight into local variances in cell response caused by concentration gradients.

Conclusions. Confocal laser scanning microscopy techniques were developed to investigate the distribution and transport of low molecular weight dyes in PEG hydrogels. The simple case of 1-D diffusion from a uniformly loaded disk was studied. Experimental data compared favorably to theoretical Fickian transport models. Diffusion coefficients on the order of 10^{-8} cm^2/s were estimated for TxR and ClN in PEG1000DA and PEG700DA, which compare favorably to literature values. Additionally, CLSM was used to monitor time-dependent molecular distributions of multiple dyes in PEG gels simultaneously. A more complex dye distribution was demonstrated and monitored with CLSM by embedding dye-loaded PEG microparticles within a PEG matrix. Control of diffusion and dye distribution was exhibited by altering the cross-linking density of the embedding matrix. The CLSM imaging techniques used in this study can be readily translated to systems with more complex geometries and dye loading as well as systems with degradable components.

Acknowledgment. This work was supported by the Packard Foundation and a GAANN fellowship to A.W.W. from the US Department of Education.

References and Notes

(1) Bryant, S. J.; Anseth, K. S. *Biomaterials* **2001**, *22*, 619−626.
(2) Burdick, J. A.; Anseth, K. S. *Biomaterials* **2002**, *23*, 4315−4323.
(3) Elisseeff, J.; McIntosh, W.; Anseth, K.; Riley, S.; Ragan, P.; Langer, R. *J. Biomed. Mater. Res.* **2000**, *51*, 164−171.
(4) Liu, V. A.; Bhatia, S. N. *Biomed. Microdevices* **2002**, *4*, 257−266.
(5) Nguyen, K. T.; West, J. L. *Biomaterials* **2002**, *23*, 4307−4314.
(6) Quick, D. J.; Anseth, K. S. *Pharm. Res.* **2003**, *20*, 1730−1737.
(7) Quick, D. J.; Anseth, K. S. *J. Controlled Release* **2004**, *96*, 341−351.
(8) Burdick, J. A.; Mason, M. N.; Hinman, A. D.; Thorne, K.; Anseth, K. S. *J. Controlled Release* **2002**, *83*, 53−63.
(9) Sawhney, A. S.; Pathak, C. P.; Hubbell, J. A. *Macromolecules* **1993**, *26*, 581−587.
(10) Metters, A. T.; Bowman, C. N.; Anseth, K. S. *J. Phys. Chem. B* **2000**, *104*, 7043−7049.
(11) Metters, A. T.; Anseth, K. S.; Bowman, C. N. *Polymer* **2000**, *41*, 3993−4004.
(12) Metters, A. T.; Anseth, K. S.; Bowman, C. N. *J. Phys. Chem. B* **2001**, *105*, 8069−8076.
(13) Bryant, S. J.; Anseth, K. S. *J. Biomed. Mater. Res., Part A* **2003**, *64A*, 70−79.
(14) West, J. L.; Hubbell, J. A. *React. Polym.* **1995**, *25*, 139−147.
(15) Lu, S.; Anseth, K. S. *Macromolecules* **2000**, *33*, 2509−2515.
(16) Mason, M. N.; Metters, A. T.; Bowman, C. N.; Anseth, K. S. *Macromolecules* **2001**, *34*, 4630−4635.
(17) Polse, K. A. *J. Am. Opt. Assoc.* **1981**, *52*, 203−208.
(18) Harvitt, D. M.; Bonanno, J. A. *Opt. Vision Sci.* **1999**, *76*, 712−719.
(19) Fatt, I.; Weissman, B. A.; Ruben, C. M. *CLAO J.* **1993**, *19*, 226−234.
(20) Compan, V.; Andrio, A.; Lopez-Alemany, A.; Riande, E.; Refojo, M. F. *Biomaterials* **2002**, *23*, 2767−2772.
(21) Lee, J.-W.; Gardella, J. A., Jr.; Hicks, W., Jr.; Hard, R.; Bright, F. V. *Pharm. Res.* **2003**, *20*, 149−152.
(22) Petersen, H.; Merdan, T.; Kunath, K.; Fischer, D.; Kissel, T. *Bioconjugate Chem.* **2002**, *13*, 812−821.
(23) Merrill, E. W.; Dennison, K. A.; Sung, C. *Biomaterials* **1993**, *14*, 1117−1126.
(24) Savas, H.; Guven, O. *Int. J. Pharm.* **2001**, *224*, 151−158.
(25) Pluen, A.; Netti, P. A.; Jain, R. K.; Berk, D. A. *Biophys. J.* **1999**, *77*, 542−552.
(26) De Smedt, S. C.; Meyvis, T. K. L.; Demeester, J.; Van Oostveldt, P.; Blonk, J. C. G.; Hennink, W. E. *Macromolecules* **1997**, *30*, 4863−4870.
(27) Burke, M. D.; Park, J. O.; Srinivasarao, M.; Khan, S. A. *Macromolecules* **2000**, *33*, 7500−7507.

(28) Heinemann, M.; Wagner, T.; Doumeche, B.; Ansorge-Schumacher, M.; Buchs, J. *Biotechnol. Lett.* **2002**, *24*, 845−850.
(29) Rafferty, D. W.; Koenig, J. L. *J. Controlled Release* **2002**, *83*, 29−39.
(30) Kazarian, S. G.; Chan, K. L. A. *Macromolecules* **2003**, *36*, 9866−9872.
(31) Belu, A. M.; Davies, M. C.; Newton, J. M.; Patel, N. *Anal. Chem.* **2000**, *72*, 5625−5638.
(32) Rajabi-Siahboomi, A. R.; Bowtell, R. W.; Mansfield, P.; Davies, M. C.; Melia, C. D. *Pharm. Res.* **1996**, *13*, 376−380.
(33) Melia, C. D.; Rajabi-Siahboomi, A. R.; Bowtell, R. W. *Pharm. Sci. Technol. Today* **1998**, *1*, 32−39.
(34) Zhang, Y.; Chu, C.-C. *J. Biomed. Mater. Res.* **2000**, *54*, 1−11.
(35) Zhang, Y.; Chu, C.-C. *J. Biomater. Appl.* **2002**, *16*, 305−325.
(36) Kang, J.; Schwendeman, S. P. *Macromolecules* **2003**, *36*, 1324−1330.
(37) Strand, B. L.; Morch, Y. A.; Espevik, T.; Skjak-Braek, G. *Biotechnol. Bioeng.* **2003**, *82*, 386−394.
(38) Stroh, M.; Zipfel, W. R.; Williams, R. M.; Webb, W. W.; Saltzman, W. M. *Biophys. J.* **2003**, *85*, 581−588.
(39) Diaspro, A., Ed. *Confocal and Two-Photon Microscopy. Foundations, Applications, and Advances*; Wiley-Liss: New York, 2002.
(40) Peppas, N. A.; Barr-Howell, B. D. In *Hydrogels in Medicine and Pharmacy*; Peppas, N. A., Ed.; CRC Press: Boca Raton, FL, 1986; Vol. 1, pp 27−56.
(41) Flory, P. J. *Principles of Polymer Chemistry*; Cornell University Press: Ithaca, NY, 1953.
(42) Anseth, K. S.; Bowman, C. N.; Brannon-Peppas, L. *Biomaterials* **1996**, *17*, 1647−1657.
(43) Canal, T.; Peppas, N. A. *J. Biomed. Mater. Res.* **1989**, *23*, 1183−1193.
(44) Crank, J. *The Mathematics of Diffusion*, 2nd ed.; Oxford University Press: New York, 1975.
(45) Russell, R. J.; Axel, A. C.; Shields, K. L.; Pishko, M. V. *Polymer* **2001**, *42*, 4893−4901.
(46) Lu, S.; Anseth, K. S. *J. Controlled Release* **1999**, *57*, 291−300.
(47) Scott, R. A.; Peppas, N. A. *Biomaterials* **1999**, *20*, 1371−1380.
(48) Elisseeff, J.; McIntosh, W.; Fu, K.; Blunk, T.; Langer, R. *J. Orthopaedic Res.* **2001**, *19*, 1098−1104.
(49) Holland, T. A.; Tabata, Y.; Mikos, A. G. *J. Controlled Release* **2003**, *91*, 299−313.

MA0475232